Environmental Science
Processes & Impacts

Accepted Manuscript

Reactivity of natural organic matter in the Florida Everglades was examined across salinity gradients and coupled with PARAFAC analysis.

Photo-reactivity of natural dissolved organic matter from fresh to marine waters in the Florida Everglades, USA

Stephen A. Timko[1]
Cristina Romera-Castillo[2]
Rudolf Jaffe[2,3]
William J. Cooper[1*]

[1]Department of Civil and Environmental Engineering
University of California, Irvine
Irvine, CA 92697-2175 USA
wcooper@uci.edu
stimko@uci.edu

[2]Florida International University
Southeast Environmental Research Center
3000 NE 151 Street
Marine Sciences Building
North Miami, Fl. 33181, USA.

[3]Department of Chemistry and Biochemistry
Florida International University
11200 SW 8th Street
Miami, FL 33199
jaffer@fiu.edu
cromerac@fiu.edu

*Corresponding Author: William J. Cooper wcooper@uci.edu

Abstract

Natural dissolved organic matter (DOM) is the major absorber of sunlight in most natural waters and a critical component of carbon cycling in aquatic systems. The combined effect of light absorbance properties and related photo-production of reactive species are essential in determining the reactivity of DOM. Optical properties and in particular excitation-emission matrix fluorescence spectroscopy combined with parallel factor analysis (EEM-PARAFAC) have been used increasingly to track sources and fate of DOM. Here we describe studies conducted in water from two estuarine systems in the Florida Everglades, with a salinity gradient of 2 to 37 and dissolved organic carbon concentrations from 19.3 to 5.74 mg C L^{-1}, aimed at assessing how the quantity and quality of DOM is coupled to the formation rates and steady-state concentrations of reactive species including singlet oxygen, hydroxyl radical, and the triplet excited state of DOM. These species were related to optical properties and PARAFAC components of the DOM. The formation rate and steady-state concentration of the carbonate radical was calculated in all samples. The data suggests that formation rates, particularly for singlet oxygen and hydroxyl radicals, are strongly coupled to the abundance of terrestrial humic-like substances. A decrease in singlet oxygen, hydroxyl radical, and carbonate radical formation rates and steady-state concentration along the estuarine salinity gradient was observed as the relative concentration of terrestrial humic-like DOM decreased due to mixing with microbial humic-like and protein-like DOM components, while the formation rate of triplet excited-state DOM did not change. Fluorescent DOM was also found to be more tightly coupled to reactive species generation than chromophoric DOM.

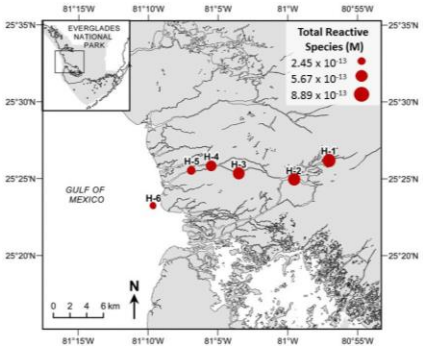

Environmental Impacts:

Reactive photo-produced species in sunlit surface waters are important in natural dissolved organic matter (DOM) cycling and contaminant degradation. Formation rates and steady-state concentrations of these species were found to be coupled to the abundance of humic-like DOM components, where terrestrial humic-like components clearly drive the DOM reactivity compared to those microbially derived. This study demonstrates the value of combining reactive species quantification techniques with excitation emission matrix fluorescence spectroscopy and parallel factor analysis modeling (EEM-PARAFAC) in order to help elucidate how changes in DOM quantity and quality affect the formation and steady-state concentrations of these species.

1. Introduction

The Everglades is one of the largest sub-tropical wetlands in the world (*ca.* 6,200 km^2), and includes extensive freshwater marsh and estuarine areas, which are characterized by open prairies and fringe mangrove swamps, respectively. Dissolved organic matter (DOM) dynamics in the Everglades are to a large extent controlled by regional soil and vegetation patterns and seasonal hydrology. Clear spatial patterns have been observed for DOM optical properties throughout the systems,[1, 2] seasonally,[3, 4] and along salinity transects in the fringe mangrove rivers.[5-7] As such, optical properties of DOM in the Everglades have been well defined and related to both physical (hydroperiod, water discharge, tidal pumping, and saltwater intrusions) and biological (primary productivity) drivers. While several studies reported on the potential effects of photo-exposure on the mineralization and degradation of chromophoric and fluorescent DOM (CDOM and FDOM, respectively) in the Shark River,[8-11] the photo-dissolution of particulate organic matter in the Everglades and Florida Bay,[12, 13] and differences in optical properties between surface and groundwater in the Everglades as a potential result of light exposure,[4] little is known about the photo-reactivity of DOM in this system and its relationship to the production of reactive species.

One of the greatest impacts of DOM on water chemistry is its role as a major source and sink of reactive photo-produced species in surface waters.[14] Singlet molecular oxygen ($^1O_2$)[15-17] and hydroxyl radical (•OH)[18] have long been understood to react with DOM[19, 20] and organic contaminants[21, 22] in sunlit surface waters. More recently, the contribution of triplet excited states of DOM (^{3}DOM*) to either enhance or inhibit the degradation of different classes of contaminants have been the subject of extensive study.[23-32] Steady-state concentrations of $^1O_2$

and ^{3}DOM* typically range on the order of ~10^{-15}-10^{-13} M in sunlit surface waters.[33] In estuarine and marine systems, the highly reactive, but much less abundant •OH (10^{-19}-10^{-16} M) reacts with bicarbonate and carbonate to form longer-lived carbonate radicals, which can be present at up to two orders of magnitude higher than •OH.[34, 35] Hydroxyl radicals can be formed from other sources as well, such as photo-Fenton reactions with iron or the photolysis of nitrate and nitrite.[18] These pathways are not as important as DOM in the Taylor- and Shark River Sloughs of the Everglades as nitrate and nitrite concentrations are well below 0.1 mg/L[36, 37] and concentrations of dissolved iron have been reported to be very low (0-0.03 mgL^{-1}).[38]

The effects of reactive species on the photodegradation of DOM are different depending on the reactant: singlet oxygen, while reacting with fulvic acids on the order of 10^{5} $M\text{-}C^{-1}s^{-1}$, does not change the DOC concentration or optical properties,[39] but can lead to partial oxidation and an increase in oxygen content[40]; ^{3}DOM* has been proposed as a major source of DOM photo-oxidation, although the mechanisms are not well understood[41]; hydroxyl radical, on the other hand, is not suspected to be a major contributor to the photodegradation of DOM due to its low formation rates,[41] although high levels of •OH formation, such as in waters with a high nitrate/DOC ratio, could lead to photomineralization.[42-44] Other reactive species, such as halide radicals, could contribute significantly to the photodegradation of DOM as well.[45] Understanding the quantity and speciation of photo-produced reactive species is therefore essential in predicting the potential for photochemical processing of organic matter, as well as contaminants, in surface waters.

There have been several studies that have looked at the changes in molecular character of DOM from fresh to marine systems.[46-50] Photolytic effects can result in a change in the overall aromatic character of the DOM[51] as well as the formation of lower molecular weight compounds,[8, 9, 52, 53] but the effect of these structural changes on reactive species photo-production are not well understood. A study of the plumes of the Mississippi and Atchafalaya Rivers in the Gulf of Mexico showed that $^{1}O_2$ production did not vary across the salinity gradient, although total free radicals decreased.[54] Due to the low DOC concentrations and detection methods, samples were ultrafiltered and concentrated through freeze-drying in order to measure reactive species production. In contrast, the organic-rich mangrove estuaries of the Everglades provide ideal study sites for conducting a detailed investigation into DOM-produced reactive species in whole waters (no preconcentration steps required) across estuarine systems, and they have been well

characterized with regards to DOM dynamics, quality, and quantity over spatial and temporal scales.[2, 3, 5, 6]

In recent years, excitation emission matrix fluorescence spectroscopy combined with parallel factor analysis modeling (EEM-PARAFAC) has been widely applied in the assessment of DOM dynamics in aquatic ecosystems. For the Everglades, a PARAFAC model has been established and applied to a variety of studies including spatial,[1, 55] and seasonal[2, 3] DOM source assessments, as well as for the estimation of source changes in the Shark River estuary.[6] The model consists of four terrestrial humic-like, two microbial humic-like and two protein-like PARAFAC components.[1, 4] Consequently, PARAFAC components in this system are well characterized and ideally suited to be applied in the development of reactivity proxies for DOM as evidenced by prior reports on potential use of two Everglades PARAFAC components as indicators of DOM light exposure.[4, 56] In this study we attempt to correlate organic matter quantity and quality using reactive species generation as the measure of photoreactivity. We present measured formation rates of singlet oxygen, ^{3}DOM*, and hydroxyl radical, and their relation to optical properties and PARAFAC components in two Everglades estuaries. Steady-state concentrations of these species as well as those calculated for carbonate radical are reported across the two systems.

2. Methods and Materials

2.1 Sample Sites

Surface water samples for this study were collected in two different estuarine regions in Everglades National Park, Florida, USA: the Shark River Slough (SRS) and Taylor Slough (TS). Estuarine inundation characteristics are quite different for these two main drainage systems for the Everglades, as the SRS is tidally influenced through the Gulf of Mexico, while the TS features no significant tidal action due to the dampening effects of the multiple mud banks throughout Florida Bay. Consequently, the mangrove swamps of the TS estuary feature longer inundation periods compared to those of the SRS, resulting in differences in mangrove forest structure, soil type (peat vs. marl) and organic matter accumulation.[57] Throughout the estuary, the freshwater slough environment is replaced by mangrove channels, tidal creeks and rivers such as the Shark and Harney rivers (for SRS) and Taylor River (for TS). Surface water samples were collected in late April 2013 (early wet season) from the Harney River and Taylor

River/Florida Bay, covering a salinity range from the oligohaline ecotone to the respective marine end-member (Fig. 1). The Harney River samples consisted of a salinity transect (six samples) covering the estuarine section between Tarpon Bay (oligo/meso-haline zone) and Ponce de Leon Bay (coastal end-member; Fig. 1a). The Taylor River samples consisted of a salinity transect along the lower Taylor River estuary (four samples) extended into Florida Bay (two samples; Fig.1b). While low salinity samples were obtained for the upper Harney River estuary, the lowest salinity sample for the Taylor River was higher at 11.2. During the late dry season (early April), saltwater intrusions from NE Florida Bay reach up into the Taylor River due to reduced freshwater head; this effect was still evident at the time of sampling.

2.2 Sample Collection

Whole water samples for reactive species analysis were collected in 1 L glass jars, stored on ice and in the dark during transport to the lab, and then stored at 4 °C until use. Samples for DOM analysis were collected in 2 L pre-washed (soaked in 0.1 M HCl and 0.1 M NaOH for 24 h each) brown Nalgene® polyethylene bottles and stored on ice until return to the lab where they were filtered through pre-combusted GF/F fiber filters prior to analysis. Salinity, temperature and pH were determined on site using a 600XL YSI probe (Xylem Inc., Yellow Springs, OH).

2.3 Reagents

Furfuryl alcohol (FFA), terephthalic acid (TPA), and sorbic acid (SA), were purchased from Sigma Aldrich (St. Louis, MO) at the highest purities available. HPLC solvents and additional reagents were purchased from Thermo Fisher Scientific, Inc. (Waltham, MA).

2.4 DOC Measurement

DOC concentrations were measured by high temperature combustion with a Shimadzu TOC-5000 analyzer. Each sample (4 mL) was acidified with 10 µL of concentrated HCl and sparged for 5 min with nitrogen to remove inorganic carbon. The mean of 3–6 injections (coefficient of variation < 2 %) was reported for each sample. The system was standardized daily with a potassium hydrogen phthalate standard.

2.5 Optical Properties

UV-Vis analyses were performed using a Varian Cary 50 Bio spectrophotometer with a 1 cm quartz cuvette, scanning from 250 nm to 800 nm. Absorption coefficients were calculated applying the equation:

$$a_{(\lambda)} = 2.303*\mathrm{abs}(\lambda)/L \quad (1)$$

where abs(λ) is the absorbance at wavelength λ, and L is the cell length in meters. Spectral slope (*S*) was obtained by fitting the absorbance spectra to the equation:

$$a_{(\lambda)} = a_{(\lambda_0)} \cdot e^{[-S\,(\lambda_0-\lambda)]} + K \quad (2)$$

where λ_0 is 250 nm and *K* is a background constant due to residual scattering by fine particle fractions or micro-air bubbles that allow for any baseline shift. Spectral slope ratio (S_R) was calculated following Helms, et al. [58] as the ratio of $S_{(275–295)}/S_{(350–400)}$. Both spectral slopes were obtained using the linear regression of the narrow wavelength ranges, $S_{(275–295)}$ and $S_{(350–400)}$, of the natural log-transformed $a_{(\lambda)}$ spectra. The carbon-specific absorption coefficient at 254 nm, $SUVA_{254}$ (expressed in L m^{-1} mg C^{-1}), was calculated by dividing the decadic a_{254} by DOC concentration.[59] UV-Vis analyses were also used to correct the inner filter effects from the fluorescence measurements.

2.6 Fluorescence and PARAFAC Analysis

Excitation-emission matrix fluorescence spectra (EEMs) were measured using a Horiba Jovin Yvon SPEX Fluoromax-3 spectrofluorometer equipped with a 150 W continuous output Xe arc lamp. Slits were set at 5.7 nm for excitation and 2 nm for emission. Forty-four emission spectral scans were acquired in a 1 cm quartz cell at excitation wavelengths (λ_{ex}) between 240 and 455 nm at 5 nm intervals. The emission wavelengths (λ_{em}) were scanned from 250 nm to 705 nm in 2 nm steps. Fluorescence signals were acquired in signal over reference ratio mode (S/R) to eliminate potential errors from fluctuations of the Xe lamp. More detailed information of post-acquisition steps for correction (inner filter effects, instrumental bias) and unit conversion to quinine sulphate units (QSU) can be found elsewhere.[4] PARAFAC modeling statistically decomposes the complex fluorescent matrix into individual, quantifiable components without any assumptions regarding their spectral shape or their number.[60] PARAFAC modeling applied here was achieved by fitting the EEMs of all the samples to an already established PARAFAC

model for surface water from the Everglades.[1, 4] Briefly, the eight components are (λ_{ex}/ λ_{em}): C1 (<260(345)/462) ubiquitous humic-like; C2 (<260/454) terrestrial humic-like possibly photo-refractory; C3 (<260(305)/416) terrestrial humic-like, fulvic acid-type; C4 (<260(305)/376) microbial humic-like; C5 (275(405)/>500) terrestrial humic-like, humic acid-type; C6 (325/406) ubiquitous humic-like, possibly generated during biodegradation, photo-labile and agricultural land use derived; C7 (275/326) and C8 (300/342) protein-like.[1,4] PARAFAC component spectral characteristics and split-half validation can be found elsewhere.[4] The analysis was carried out in MATLAB 7.0.4. (Mathworks, Natick, MA) with the DOMFluor toolbox.[61]

2.7 Irradiation Experiments

Irradiation experiments were carried out in a Luzchem SolSim solar simulator (Ottawa, Canada). The output of the 300W ceramic Xe lamp was adjusted with a 1/8" Esco optical glass filter and dimmer to best match the AM 1.5 solar spectrum with irradiation from 300 nm- 900 nm. Lamp output was measured daily with the Reliability Direct (League City, Texas) AR823 power meter that comes standard with the system. The sample chamber was well-ventilated, keeping the samples at a constant 20°C. Samples were placed in sealed quartz cells (1 cm path length) on a rotating sample holder to ensure even irradiation. Aliquots were taken at intervals ranging from 5-30 minutes, and the samples analyzed by HPLC with on-line UV or fluorescence detection.

2.8 Hydroxyl and Carbonate Radicals

Hydroxyl radical formation and steady-state concentrations were monitored using terephthalic acid (TPA).[62] To measure the rate of •OH production, each sample was adjusted to pH<2 with HCl and bubbled with air to strip off any (bi)carbonate in the system. The samples were raised back to the original pH with NaOH and spiked with TPA (6 μM final concentration). Formation of 2-hydroxyterephthalic acid, 2HTPA, is described by Equation 3:

$$\frac{d[\mathrm{2HTPA}]}{dt} = k_{\cdot\mathrm{OH,TPA}} Y [\mathrm{TPA}][\bullet\mathrm{OH}]^*_{ss} \qquad (3)$$

where $k_{\cdot\mathrm{OH,TPA}}$= 4.4 x 10^9 M^{-1} s^{-1}, the yield Y = 0.35, and $[\bullet\mathrm{OH}]^*_{ss}$ is the steady-state concentration of •OH in carbonate-free solutions. Formation rates of •OH, $R_{\cdot\mathrm{OH}}$, were calculated

by dividing the rate of 2HTPA formation by the reaction yield. While 2HTPA is subject to photolysis by light below 360 nm, no loss of 2HTPA was seen in irradiations <100 min, so in order to keep the light source constant between experiments, no additional filters were added to the lamp for •OH measurements. Whole water $[\bullet OH]_{ss}$ were then determined with Equation 4:

$$[\bullet OH]_{ss} = \frac{R_{\cdot OH}}{k_{\cdot OH,HCO_3^-}[HCO_3^-] + k_{\cdot OH,CO_3^{2-}}[CO_3^{2-}] + k_{\cdot OH,DOM}[DOM]} \quad (4)$$

with the reaction rates between hydroxyl radical and bicarbonate and carbonate ($k_{\cdot OH,HCO_3^-}$ = 8.50 x 10^6 M^{-1} s^{-1}, and $k_{\cdot OH,CO_3^{2-}}$ = 3.9 x 10^8 M^{-1} s^{-1} , respectively),[63] and the reaction rate with DOM, $k_{\cdot OH,DOM}$, calculated as the average of the values for organic matter determined by Westerhoff, et al. [20] (excluding effluent organic matter), (1.4 ± 0.2) x 10^4 L (mg C)$^{-1}$ s^{-1}. Bicarbonate and carbonate concentrations were determined with a Metrohm 855 Robotic Titrosampler (Riverview, FL). Carbonate radical concentrations were calculated with the following equation:

$$[CO_3^{\cdot-}]_{ss} = \frac{\left[k_{\cdot OH,HCO_3^-}[HCO_3^-] + k_{\cdot OH,CO_3^{2-}}[CO_3^{2-}]\right][\bullet OH]^*_{ss}}{k_{CO_3^{\cdot-},DOM}[DOM]} \quad (5)$$

where $k_{CO_3^{\cdot-},DOM}$ = 280 ± 90 L (mg C)$^{-1}$ s^{-1}.[35] Carbonate radicals are also produced by the reaction between carbonate ions with triplet excited state DOM, but the reaction rate (1 x 10^5 M s^{-1})[35] is such that the contribution of ^{3}DOM* to carbonate radical formation was negligible. Due to long-term monitoring data that has consistently shown low (<0.1 mg/L) concentrations of nitrate and nitrite,[36, 37] these species were not measured. Dissolved iron concentrations were not determined, but have been reported to be low in the Everglades (0-0.03 mg/L). In addition, total Fe concentrations in Everglades' soils and sediments have been reported to be low (http://fcelter.fiu.edu/), and sulfate reducing conditions in the ecotonal fringe mangrove sediments further limit iron solubility due to the formation of insoluble sulfides.[64] All •OH production was therefore attributed to DOM.

2.9 Singlet Oxygen

Steady-state concentrations of singlet oxygen were determined using furfuryl alcohol (FFA) as a probe.[65] Water samples were spiked with FFA (1.5 mM final concentration), placed

in the solar simulator, and aliquots taken every 10 minutes. The concentration of FFA was plotted versus time to determine the initial rate of FFA loss, R_{FFA}. The rate of $^1O_2$ production was then determined by incorporating the deactivation of $^1O_2$ due to solvent effects, $k_d = 2.5 \times 10^5\ s^{-1}$,[66] with Equation 6 [67]:

$$R_{^1O_2} = R_{FFA}\ \frac{k_{FFA,\ ^1O_2}\mathrm{FFA}_0 + k_d}{k_{FFA,\ ^1O_2}\mathrm{FFA}_0} \tag{6}$$

where FFA_0 is the initial FFA concentration and $k_{FFA,\ ^1O_2}$ is the reaction rate between FFA and $^1O_2$, $1.2 \times 10^8\ M^{-1}\ s^{-1}$.[65] While there is potential for error due to reaction with hydroxyl radical ($k_{FFA,\cdot OH} = 1.2 \times 10^{10}$)[63], $R_{\cdot OH} << R_{^1O_2}$, making the contribution of hydroxyl radical negligible. Steady-state concentrations in the absence of the probe were determined by dividing the formation rate by k_d:

$$[\,^1O_2]_{ss} = \frac{R_{^1O_2}}{k_d} \tag{7}$$

2.10 Triplet Excited State of DOM (^{3}DOM)*

^{3}DOM* formation was measured with sorbic acid as described in Grebel et al.[68] 2,4,6-trimethylphenol (TMP) was not used as a probe due to changes in its reaction rate with ^{3}DOM* at varying ionic strengths.[69] Formation rates of the cis-trans isomer of sorbic acid were divided by the yield, 0.18, to obtain the removal rate of ^{3}DOM* by sorbic acid, R_{SA}. The concentration of the probe, [SA], divided by R_{SA} was plotted against the concentration of the probe:

$$\frac{[SA]}{R_{SA}} = \frac{[SA]}{R_{^3DOM^*}} + \frac{k_s'}{R_{^3DOM^*} k_{SA,\ ^3DOM^*}} \tag{8}$$

where $R_{^3DOM^*}$ is the formation rate of triplets, k_s' is the reaction rate of solution scavengers with the triplets (inverse of triplet lifetimes), and $k_{SA,\ ^3DOM^*}$ is the reaction rate between sorbic acid and ^{3}DOM*, calculated as the average of reported values between sorbic acid and various organic matters, $(3.35 \pm 1.00) \times 10^9\ M^{-1}\ s^{-1}$.[70] Formation rates of triplets were therefore calculated as the inverse of the slope, while k_s' and steady-state concentrations, $[^3DOM^*]_{ss}$, (in the absence of probe) were determined as follows:

$$k_s' = k_{SA,\ ^3DOM^*} \cdot \frac{\text{intercept}}{\text{slope}} \tag{9}$$

$$[^3DOM^*]_{ss} = \frac{R_{^3DOM^*}}{k_s'} \tag{10}$$

2.11 Analytical Methods

Probe compounds were quantified using an Agilent 1200 Series HPLC with UV detection at wavelengths 254 nm for TPA and SA and 219 nm for FFA. Formation of 2HTPA was monitored using on-line fluorescence, λ_{ex} = 240 nm, λ_{em} = 425 nm. The isocratic mobile phase for TPA/2HTPA detection was 50:50 0.08% H_3PO_4:methanol. The remaining compounds used 30 mM sodium acetate buffer at pH=4.75 with ratios of 90:10 acetate:methanol for FFA, and 85:15 acetate:acetonitrile for SA. FFA was monitored using a Phenomenex Gemini 3µm C18 column (50 x 4.6 mm i.d.), while TPA and SA were monitored using a Phenomenex Gemini 5µm C18 column (250 x 4.6 mm i.d.).

3. Results

3.1 DOC distribution

Samples along the Harney River and the Taylor Slough showed decreasing DOC with increasing salinity (Table 1), which was expected due to the dilution of freshwater marsh-derived DOC with the marine end-members. The observed decrease in the Harney River shows non-conservative mixing indicative of DOC contributions from the fringe mangroves as previously reported.[6] The Taylor Slough, with minimal tidal activity and significantly lower freshwater discharge compared to the Harney, did not show this same trend. However, as mentioned above, low-salinity samples of the Taylor River were not obtained due to the low-discharge conditions during time of sampling, and the two high salinity end-member points of the Taylor Slough sample set were taken in Florida Bay (Fig. 1b). Since these samples are not part of a spatial, riverine salinity transect, the DOC origin in the TS sample set cannot be exclusively linked to the Taylor River, and the apparent conservative mixing trend cannot be confirmed. The changes in DOC concentration along the salinity gradient in these two systems were nonetheless quite similar, allowing for a comparison of formation rates and steady-state concentrations of reactive species between the Harney River and Taylor River/Florida Bay estuaries.

3.2 Optical properties and PARAFAC analysis

Optical properties for the twelve sample sites are summarized in Table 2. The distribution of CDOM as indicated by a_{254} was in general agreement with the DOC concentrations in both systems. The Harney River was enriched significantly with CDOM compared to the Taylor River sample set. This is, in part, due to the fact that the DOM loadings to the Taylor River are

enriched in microbial sources,[2] particularly during the end of the dry season, when intrusions of Florida Bay waters upriver are prominent. Waters from Florida Bay are enriched in seagrass-derived DOM and therefore feature higher abundances in carbohydrates and proteins (protein-like fluorescence) compared to the humic-like materials and lignins found in the SRS mangrove rivers such as the Harney River.[3, 5] The higher $SUVA_{254}$ values and PARAFAC component fluorescence confirm these differences in DOM source and character between the two systems (Table 2). Fluorescent PARAFAC components showed a similar behavior to DOC, with a decrease of the fluorescent intensity with the increase of salinity. Humic-like components C1, C3, C4, C5 and C6 and the protein-like C7 presented a non-conservative behavior, showing clear DOM contributions from the fringe mangrove swamps (values above the theoretical conservative mixing line)[6]; however, humic-like C2 and protein-like C8 showed a nearly conservative behavior. In all the cases, fluorescent intensity values of Harney River were higher than that of Taylor Slough. In terms of abundance (percent total fluorescence), the Harney was enriched in terrestrial humic-like components C1 ($p<0.005$), C3 ($p<0.01$), and C5 ($p<0.05$), while the Taylor was enriched in microbial humic-like C4 ($p<0.05$), and protein-like C7 ($p<0.005$) and C8 ($p<0.001$). DOC and PARAFAC results from the Harney River agree with those previously observed for the same season.[56] Spectral slope ratios (S_R), an established proxy for DOM molecular weight (MW),[58] showed a general trend of decreasing MW (increasing S_R) with increasing salinity (Table 2). This is expected due to the formation of lower MW DOM compounds due to photobleaching[71] as well as the predominance of lower molecular weight autochthonous material at the marine end-member sites. Sample H1, the uppermost and most freshwater-influenced sample of the Harney River, showed lower MW compared to the oligohaline zone samples due to contributions of periphyton-derived DOM (lower MW) from the freshwater marshes.[2] DOM from the most saline site of the Taylor Slough, T6, showed a slightly higher MW (lower S_R) than the preceding estuarine sites. This site is located in a region of the bay that has low water exchange and consequently high residence times. It is also in a zone of high seagrass mortality and associated detritus. Bio- and photo-polymerization reactions could therefore be responsible for the MW increase seen in this region.

3.3 Reactive Species

Normalized formation rates and steady-state concentrations for the four photo-produced reactive species are shown in Figures 2 and 3. Formation rates and steady-state concentrations of

singlet oxygen (normalized to DOC concentration) decreased ($p<0.01$) in the Harney River by only 13 % across the salinity gradient, compared to the Taylor Slough sites, which decreased ($p<0.01$) by 56 % (Fig. 2a, 3a). Formation rates and steady-state concentrations of ^{3}DOM* normalized to DOC did not change significantly along the two transects (Fig. 2b, 3b). The average normalized formation rates of ^{3}DOM* for the Harney River and Taylor Slough were 4.80×10^{-9} and 3.38×10^{-9} M s^{-1} (mg C/L)$^{-1}$, respectively, while the average normalized steady-state concentrations were 2.55×10^{-14} and 1.26×10^{-14} M (mg C/L)$^{-1}$, respectively. The decrease in normalized formation rates of •OH (Fig. 2c) was much greater than the decrease in singlet oxygen, and was similar in the two systems: 90 % in the Harney River and 87 % in the Taylor Slough. The normalized steady-state concentrations decreased by 75 % and 71 %, respectively (Fig. 3c). This trend is likely due to both the loss of DOM as well as decreasing bicarbonate and carbonate concentrations along transects (Table 2), resulting in less scavenging and therefore higher relative steady-state concentrations. The soils of the Everglades contain significant amounts of calcareous periphyton remains. Dissolution of these carbonates results in the fresher waters having higher bicarbonate and carbonate (total alkalinity) concentrations than the marine end-member, particularly for the Harney River. The gradient was less steep for the Taylor system as the marine end-member, Florida Bay, is characterized by calcareous mud sediments. Normalized carbonate radical formation rates therefore decreased by 91 % and 88 % and normalized steady-state concentrations decreased by 72 % and 70 % and along the transects of the Harney and Taylor Rivers, respectively, as the major reactants decreased.

4. Discussion

4.1 Reactive species

In a recent study, Parker et al.[69] reported an increase in ^{3}DOM* lifetimes and therefore steady-state concentrations of ^{3}DOM* with increasing ionic strength. These results are supported in the present study, as normalized ^{3}DOM* lifetimes increased in the Harney river until the marine end-member, where a significant increase in the abundance of protein-like C7 and C8 and microbial humic-like C4 and decrease in terrestrial humic-like C1 and C5 was observed (Fig. S1). The Taylor River did not show a significant change in normalized $[^3\text{DOM}^*]_{ss}$ across the salinity gradient, possibly due to a balance between the loss of ^{3}DOM* due to marine end-member dilution with an increase of ^{3}DOM* lifetimes. It should be noted that the high

uncertainties in the steady-state concentrations (~30 %) are due mainly to the uncertainty associated with the estimation of the rate constant between SA and ^{3}DOM* (Equations 9, 10). Experimental error in determining the formation rates were much lower (<10 %), as evident in Table 3.

Previous studies showed that increases in ionic strength do not affect $[^1O_2]_{ss}$,[54, 69] suggesting that changes in $^1O_2$ production along a salinity transect and between the two sites were due to changes in the quality of the DOM. The ratios of formation rates of $^1O_2$ and ^{3}DOM*, $R_{^1O_2}/R_{^3DOM^*}$, ranged from 0.76-1.40 in the Harney River, and from 0.48-1.28 in the Taylor Slough. While it may seem counter-intuitive that at some sites $^1O_2$ is forming faster than its precursor, ^{3}DOM*, the ^{3}DOM* formation reported only accounts for ^{3}DOM* with triplet energies ≳250 kJ mol^{-1} necessary to react with sorbic acid, while the energy required to excite ground-state molecular oxygen to $^1O_2$ is only 94 kJ mol^{-1}. These high-energy triplets- on average, 35 % of total triplets- possess the range of energies required for triplets to react with many contaminants, making the reported formation rates and steady-state concentrations relevant for calculating environmental fate of contaminants.[33] The decrease in $^1O_2$ formation across the transects could be due to the loss of either oxygen in the system or ^{3}DOM* with triplet energies between 94 and 250 kJ mol^{-1}, as $R_{^3DOM^*}$ did not vary significantly across either system. While the solubility of oxygen decreases with increasing salinity, if the loss of O_2 was the cause of the decrease in $^1O_2$, the Harney River would theoretically show greater $^1O_2$ decrease than the Taylor Slough as the salinity range was greater. As this was not the case- decrease in the Harney was only 13 %, compared to 56 % in the TS- this mechanism is unlikely. No evidence of significant bio- or photodegradation of the DOM was found in the optical properties or PARAFAC analysis, in support of the latter mechanism. Therefore, the most likely cause for changes in $^1O_2$ is the change in DOM quality resulting from increased contributions of DOM from the marine end-member. This is evident from the data shown in Table 2, where optical properties indicative of higher abundance of humic-like substances and aromaticity such as a_{254}, $SUVA_{254}$ and the relative abundance of the terrestrial humic-like PARAFAC components (C1, C3 and C5) were enriched in the Harney compared to the Taylor estuarine samples, and also changed along the salinity transect with lower a_{254} and humic-like fluorescence and higher protein-like fluorescence at higher salinities. Grandbois, et al. [72] showed that a microbial-derived DOM isolate (Pony Lake Fulvic Acid) has lower formation rates of $^1O_2$ than a terrestrial-derived DOM isolate (Suwannee

River Humic Acid), and that the ratio of steady-state concentrations constrained in the DOM micelles to that in the bulk solution were higher in microbial-derived DOM by over a factor of seven. These results support the hypothesis that changes in DOM source from terrestrial to microbial were the main drivers behind the measured changes in $^1O_2$ formation.

While the effects of ionic strength on ^{3}DOM* and $^1O_2$ production were shown to be non-halide-specific,[69] at constant ionic strength, chloride and bromide concentrations do affect the production of these species as well as •OH.[73] The influence of ionic strength on the production of •OH is not known, although halides are known quenchers of •OH. While the loss of •OH to halides, namely bromide, could have influenced the measured formation rates in this study, it is believed that these effects were minimal due to the high solution pH; however, the reduction in quantum yield of production of •OH by halides may have contributed to the decreased formation rates measured.[73] More research is needed to determine the mechanism of •OH formation so that the effects of ionic strength as well as halides can be better understood.

Relationships between formation rates of reactive species and optical properties and PARAFAC results were investigated in place of steady-state concentrations as formation of reactive species is dependent on DOM composition, while steady-state concentrations are heavily dependent on the presence of solution scavengers. No attempt was made to correlate formation rates of carbonate radical with optical properties or PARAFAC components as the majority of formation results from reactions with the hydroxyl radical and is not directly formed as a result of DOM photochemistry.

4.2 Optical properties and reactive species

Photodegradation of DOM has previously been shown to decrease not only the average molecular weight of the DOM,[71] but also the reactive species production.[41] In this dataset, as the spectral slope ratios increased (higher S_R values are indicative of lower molecular weights), nonlinear decreases in reactive species formation rates were observed when considering the entire, combined dataset (Fig. S2). However, when considering the individual data for the two systems, no clear trend was observed. Multiple studies have shown that the smaller size fractions of DOM are more efficient at producing reactive species.[54, 67, 74-76] These results come from the size fractionation of individual DOM sources through filtration or size exclusion chromatography. While the smallest size fractions of a single DOM sample may be the most

photoreactive, changes in S_R in this study more likely represent bulk MW changes across the sample sites than photodegradation products. They are a result of changing DOM quality from enriched soil/terrestrial sources at the freshwater end-member to microbial/autochthonous source enriched DOM at the marine end-member. The decreased reactive species formation rates with increasing S_R are consequently caused by a gradual shift (estuarine mixing) of more humic-like, higher MW DOM to less humic-like, lower MW DOM along the salinity gradient. This source change and associated DOM quality change is clearly reflected in its reactivity.

The absorbance at 254 nm, a_{254}, had a positive linear relationship (R^2=0.959) with singlet oxygen production (Fig. 4a), which is in agreement with previous studies.[77] $SUVA_{254}$, an established proxy for aromaticity,[59] increased linearly with formation rates of $^1O_2$ in the Taylor Slough (R^2=0.980) , but was only modestly correlated to the formation rates of $^1O_2$ in the Harney River (R=0.499) (Fig 5a) possibly due to the DOM quality variations resulting from mangrove swamp contributions (non-conservative behavior) for the mid-salinity range. Formation rates of ^{3}DOM* showed a strong positive correlation to a_{245} (R= 0.855) and modest positive correlation to $SUVA_{254}$ (R=0.659) (Fig. 4b, 5b). While it may seem surprising that the correlation to $SUVA_{254}$, and by association aromaticity, was not stronger as aromatic ketones [23-25, 78, 79] and quinones [78-80] are thought to be major sources of triplet excited states found in DOM, quinones may play a lesser role in DOM optical properties [81] and therefore, the contributions of quinones to ^{3}DOM* formation would not necessarily be captured by the $SUVA_{254}$ measurement. Formation rates of hydroxyl radical in the Taylor Slough sample set showed a very strong correlation to a_{245} (R=0.995), while the Harney River rates showed a less strong correlation (R=0.740) (Fig 4c). Taylor Slough showed a very strong correlation between $R_{\cdot OH}$ and $SUVA_{254}$ (R=0.984), while the Harney River showed a very weak correlation (R=0.171) (Fig. 5c). This suggests that aromaticity may be more important for hydroxyl radical generation in microbial and seagrass-derived DOM than in terrestrial humic-like DOM, a result that merits further study, as the mechanisms of hydroxyl radical photo-production by DOM is poorly understood.[42] Seagrass- derived DOM has been reported to be enriched in non-lignin polyphenols [5] which may be important in this process.

4.3 PARAFAC and reactive species

The relationships between reactive species formation rates and the fluorescence intensity of the PARAFAC components were investigated to examine the potential for use of fluorescence as a proxy for reactive species formation. Excellent linear correlations between $^1O_2$ and PARAFAC components were observed (R^2 = 0.916-0.976) for both Harney and Taylor rivers and for all PARAFAC components (Fig. 6), suggesting that FDOM is a comparable proxy for $^1O_2$ formation to a_{254} (R^2= 0.959) and superior to $SUVA_{254}$ (R^2 = 0.701). For the Harney River, the correlation with C2 does not visually seem linear. While the reason for this difference is not clear, this component has been proposed to be photo-stable or a product of photo-degradation,[4,55] which may affect its potential to generate reactive species. Similarly, excellent linear correlations were observed between •OH formation rates and PARAFAC components (other than C2) in the Taylor River (R^2 = 0.854-0.991; Fig. S3), while the relationship appeared nonlinear in the Harney River. Formation rates of ^{3}DOM* and PARAFAC component fluorescence were less correlated (R^2 = 0.558-0.839; Fig. S4).

The relationships between the DOC-normalized formation rates of reactive species with respect to the relative abundance of the PARAFAC components (% FDOM) were examined as well. In general, $^1O_2$ showed positive relationship to the relative abundance of terrestrial humic-like PARAFAC components C1, C3, and C5 and a negative relationship to percent of protein-like components C7 and C8 and microbial humic-like C4 (and C6 for Taylor; Fig 7). These data suggest that moieties present in the terrestrial humic substances are the main source of $^1O_2$ in the bulk waters, with other fractions of the DOM playing a smaller role. The change in $[^1O_2]_{ss}$ with the abundance of terrestrial or microbial PARAFAC components in the Harney River was significantly lower than in the Taylor Slough, probably as a result of a significantly stronger DOM quality gradient in the latter system. The influence of microbial and seagrass-derived DOM in the Taylor samples is clearly reflected by a reduction in its photochemical reactivity compared to the DOM in the Harney. While •OH formation showed a similar relationship with PARAFAC components relative abundance (Fig. S5), ^{3}DOM* formation did not show a strong correlation to the abundance of any individual PARAFAC component (Fig. S6). This is not unusual, as there was not a significant change in ^{3}DOM* formation rates across the two systems. The strongest correlations were modest negative correlations with the two protein-like components, C7 (R= -0.646) and C8 (-0.617), followed by modest positive correlations to terrestrial humic-like C5 (R= 0.560), C1 (R=0.553) and C3 (R=0.530)

As mentioned previously, the mechanisms of hydroxyl radical photoproduction by DOM are poorly understood.[42] Similar to $^1O_2$, absolute formation rates of the hydroxyl radical showed positive correlation to the absolute fluorescence of each of the PARAFAC components, while the normalized formation rates showed positive correlation to abundance of terrestrial humic-like components C1, C3, and C5, and negative correlation to microbial humic-like C4, and C6, and the protein-like C7 and C8 (Fig. S4). These relationships highlight the importance of caution when attempting to correlate quantitative and qualitative PARAFAC component information with photoreactivity of DOM: for example, simply looking at the relationship between absolute formation rates of •OH and C8 fluorescence would give the impression that the two have a strong positive correlation, while examining the normalized formation rate versus the abundance of C8 shows an exponential decrease in •OH formation with higher C8 abundance. Thus, while the abundance of FDOM is clearly a driver for reactive species formation rates, it is ultimately the DOM quality (allochthonous vs. autochthonous) which is critical in this formation process. As such, the relative abundance of terrestrial, humic-like PARAFAC components could serve as a proxy for the potential for reactive species generation, particularly for $^1O_2$.

Conclusions

Formation rates and steady-state concentrations of singlet oxygen, triplet excited-state DOM, and hydroxyl radical were determined for two different estuarine transects of the Florida Everglades. Carbonate radical formation rates and steady-state concentrations were calculated from the hydroxyl radical and alkalinity data. Both formation rates and steady-state concentrations were directly related to CDOM, $SUVA_{254}$ and FDOM, but were clearly driven by the relative abundance of terrestrial humic-like DOM components, while they correlated negatively with the microbial humic-like and protein-like components of DOM. This is in agreement with a study of Arctic waters that similarly showed a positive correlation of •OH formation to terrestrial organic matter fluorescence and a negative correlation to protein-like fluorescence [82] as well as a previous study that showed higher $[^1O_2]_{ss}$ in bulk solutions from terrestrial-derived DOM compared to microbial-derived DOM.[72] Singlet oxygen formation rates and steady-state concentrations (normalized to DOC) decreased slightly in the Harney River and more so in the Taylor Slough along the salinity gradient, most likely due to changes in the abundance of humic-like substances along the salinity gradient, and due to differences in

dissolved organic matter quality (microbial vs. terrestrial) between the two estuarine systems. Normalized formation rates and steady-state concentrations of ^{3}DOM* were found not to change significantly along the salinity gradients. Hydroxyl radical formation (normalized to DOC) decreased by >87 % across the transects of both systems, and showed similar relationships to DOM as singlet oxygen, with higher production in waters with a higher abundance of terrestrial humic-like components and decreased production in waters with higher abundance of microbial humic-like and protein-like DOM. A strong correlation between •OH formation and $SUVA_{245}$, an established proxy for aromaticity, was seen in the Taylor Slough samples, but not in the Harney River, suggesting that aromaticity may be more important in •OH formation from microbial/autochthonous DOM than terrestrial-derived DOM. Carbonate radical decreased along the transects as well, as its major precursor is •OH.

This study demonstrates the strength of combining reactive species measurements with DOM optical properties as a means to assess environmental drivers and molecular controls on DOM reactivity in aquatic environments. PARAFAC analysis has been demonstrated as a useful tool to qualitatively assess the contributions of different organic matter components to the photo-production of reactive species. The correlations between FDOM and reactive species production are to be expected: fluorescent emissions are generated by excited singlet states of DOM, which are the precursors of ^{3}DOM*, the main source of $^1O_2$ in sunlit natural waters. Recent work has also shown that electron transfer from excited singlet states could form intermediates that produce superoxide.[83] Additional research is needed on greater spatial and temporal scales to be able to use PARAFAC analyses to not only determine reactive species source, but also as quantitative proxies for the estimation of reactive species potential as a measure of DOM photoreactivity.

Acknowledgments - The authors thank the Southeast Environmental Research Center (SERC) at FIU for providing partial funds through the Eminent Scholars Program to WJC in support of this study and field logistics. This work was partially funded through NSF grants DBI 0220409 (FCE LTER) and CBET-1034555 to RJ and WJC, respectively. RJ thanks SERC for additional support through the George Barley Endowment. CRC thanks Generalitat de Catalunya for support through the Postdoctoral Beatriu de Pinós Fellowship. This material is based upon work supported by the National Science Foundation Graduate Research Fellowship Program under

Grant No. DGE-1321846 (SAT). This is contribution number 649 from the Southeast Environmental Research Center.

References

1. Y. Yamashita, L. J. Scinto, N. Maie and R. Jaffe, *Ecosystems*, 2010, **13**, 1006-1019.
2. M. Chen, N. Maie, K. Parish and R. Jaffé, *Biogeochemistry*, 2013, **115**, 167-183.
3. N. Maie, Y. Yamashita, R. M. Cory, J. N. Boyer and R. Jaffé, *Appl. Geochem.*, 2012, **27**, 917-929.
4. M. Chen, R. M. Price, Y. Yamashita and R. Jaffe, *Appl. Geochem.*, 2010, **25**, 872-880.
5. N. Maie, C. Y. Yang, T. Miyoshi, K. Parish and R. F. Jaffe, *Limnol Oceanogr*, 2005, **50**, 23-35.
6. K. M. Cawley, Y. Yamashita, N. Maie and R. Jaffé, *Estuaries and Coasts*, 2013, 1-12.
7. R. Jaffe, J. N. Boyer, X. Lu, N. Maie, C. Yang, N. M. Scully and S. Mock, *Mar. Chem.*, 2004, **84**, 195-210.
8. E. Zanardi-Lamardo, C. D. Clark, C. A. Moore and R. G. Zika, *Environ. Sci. Technol.*, 2002, **36**, 2806-2814.
9. E. Zanardi-Lamardo, C. A. Moore and R. G. Zika, *Mar. Chem.*, 2004, **89**, 37-54.
10. C. D. Clark, W. T. Hiscock, F. J. Millero, G. Hitchcock, L. Brand, W. L. Miller, L. Ziolkowski, R. F. Chen and R. G. Zika, *Mar. Chem.*, 2004, **89**, 145-167.
11. C. D. Clark, J. Jimenez-Morais, G. Jones, E. Zanardi-Lamardo, C. A. Moore and R. G. Zika, *Mar. Chem.*, 2002, **78**, 121-135.
12. O. Pisani, Y. Yamashita and R. Jaffe, *Water Res.*, 2011, **45**, 3836-3844.
13. G. C. Shank, A. Evans, Y. Yamashita and R. Jaffe, *Limnol Oceanogr*, 2011, **56**, 577-588.
14. W. J. Cooper, R. G. Zika, P. R. G. and A. M. Fischer, in *Influence of Aquatic Humic Substances on Fate and Treatment of Pollutants*, eds. P. MacCarthy and I. H. Suffet, American Chemical Society, Editon edn., 1989, pp. 333-362.
15. R. G. Zepp, N. L. Wolfe, G. L. Baughman and R. C. Hollis, *Nature*, 1977, **267**, 421-423.
16. W. R. Haag, J. Hoigne, E. Gassman and A. M. Braun, *Chemosphere*, 1984, **13**, 641-650.
17. C. Shao, W. J. Cooper and D. R. S. Lean, in *Aquatic and Surface Photochemistry*, eds. G. R. Helz, R. G. Zepp and D. G. Crosby, Lewis Publishers, Boca Raton, FL, Editon edn., 1994, pp. 215-221.
18. O. C. Zafiriou, *Journal of Geophysical Research*, 1974, **79**, 4491-4497.
19. N. M. Scully, W. J. Cooper and L. J. Tranvik, *FEMS Microbiology Ecology*, 2003, **46**, 353-357.
20. P. Westerhoff, S. P. Mezyk, W. J. Cooper and D. Minakata, *Environ. Sci. Technol.*, 2007, **41**, 4640-4646.
21. R. Andreozzi, R. Marotta and N. Paxeus, *Chemosphere*, 2003, **50**, 1319-1330.
22. A. L. Boreen, W. A. Arnold and K. McNeill, *Aquatic Sciences - Research Across Boundaries*, 2003, **65**, 320-341.
23. S. Canonica, B. Hellrung, P. Müller and J. Wirz, *Environ. Sci. Technol.*, 2006, **40**, 6636-6641.
24. S. Canonica, B. Hellrung and J. Wirz, *The Journal of Physical Chemistry A*, 2000, **104**, 1226-1232.
25. S. Canonica, U. Jans, K. Stemmler and J. Hoigne, *Environ. Sci. Technol.*, 1995, **29**, 1822-1831.
26. S. Canonica and H.-U. Laubscher, *Photochemical & Photobiological Sciences*, 2008, **7**, 547-551.
27. J. Wenk and S. Canonica, *Environ. Sci. Technol.*, 2012, **46**, 5455-5462.
28. J. Wenk, U. von Gunten and S. Canonica, *Environ. Sci. Technol.*, 2011, **45**, 1334-1340.
29. H. M. Xu, W. J. Cooper, J. Jung and W. H. Song, *Water Res.*, 2011, **45**, 632-638.
30. X. Z. Luo, Z. Zheng, J. Greaves, W. J. Cooper and W. H. Song, *Water Res.*, 2012, **46**, 1327-1336.
31. H. Santoke, W. H. Song, W. J. Cooper and B. M. Peake, *J. Hazard. Mater.*, 2012, **217**, 382-390.
32. L. Wang, H. M. Xu, W. J. Cooper and W. H. Song, *Sci. Total Environ.*, 2012, **426**, 289-295.
33. R. G. Zepp, P. F. Schlotzhauer and R. M. Sink, *Environ. Sci. Technol.*, 1985, **19**, 74-81.
34. B. Sulzberger, S. Canonica, T. Egli, W. Giger, J. Klausen and U. von Gunten, *Chimia*, 1997, **51**, 900-907.
35. S. Canonica, T. Kohn, M. Mac, F. J. Real, J. Wirz and U. Von Gunten, *Environ. Sci. Technol.*, 2005, **39**, 9182-9188.

36. D. L. Childers and T. G. Troxler, ed. L. T. E. R. Network, Editon edn., 2013.
37. D. L. Childers and T. G. Troxler, ed. L. T. E. R. Network, Editon edn., 2013.
38. M. M. Reddy, G. Aiken, P. F. Schuster, C. Gunther, S. Charlton and J. Tregellas, *Summary of data from onsite and laboratory analyses of surface water and marsh porewater from South Florida Water Management District water conservation areas, the Everglades, South Florida*, USGS, 1995.
39. R. M. Cory, J. B. Cotner and K. McNeill, *Environ. Sci. Technol.*, 2009, **43**, 718-723.
40. R. M. Cory, K. McNeill, J. P. Cotner, A. Amado, J. M. Purcell and A. G. Marshall, *Environ. Sci. Technol.*, 2010, **44**, 3683-3689.
41. S. Loiselle, D. Vione, C. Minero, V. Maurino, A. Tognazzi, A. M. Dattilo, C. Rossi and L. Bracchini, *Water Res.*, 2012, **46**, 3197-3207.
42. D. Vione, G. Falletti, V. Maurino, C. Minero, E. Pelizzetti, M. Malandrino, R. Ajassa, R.-I. Olariu and C. Arsene, *Environ. Sci. Technol.*, 2006, **40**, 3775-3781.
43. T. Brinkmann, P. Hörsch, D. Sartorius and F. H. Frimmel, *Environ. Sci. Technol.*, 2003, **37**, 4190-4198.
44. J. V. Goldstone, M. J. Pullin, S. Bertilsson and B. M. Voelker, *Environ. Sci. Technol.*, 2002, **36**, 364-372.
45. J. E. Grebel, J. J. Pignatello, W. Song, W. J. Cooper and W. A. Mitch, *Mar. Chem.*, 2009, **115**, 134-144.
46. M. Gonsior, B. M. Peake, W. T. Cooper, D. Podgorski, J. D'Andrilli and W. J. Cooper, *Environ. Sci. Technol.*, 2009, **43**, 698-703.
47. M. Gonsior, B. M. Peake, W. T. Cooper, D. C. Podgorski, J. D'Andrilli, T. Dittmar and W. J. Cooper, *Mar. Chem.*, 2011, **123**, 99-110.
48. M. A. Moran, W. M. Sheldon and R. G. Zepp, *Limnol Oceanogr*, 2000, **45**, 1254-1264.
49. R. L. Sleighter and P. G. Hatcher, *Mar. Chem.*, 2008, **110**, 140-152.
50. A. Stubbins, R. G. M. Spencer, H. Chen, P. G. Hatcher, K. Mopper, P. J. Hernes, V. L. Mwamba, A. M. Mangangu, J. N. Wabakanghanzi and J. Six, *Limnol Oceanogr*, 2010, **55**, 1467-1477.
51. A. Stubbins, J. Niggemann and T. Dittmar, *Biogeosciences*, 2012, **9**, 1661-1670.
52. K. Mopper, X. L. Zhou, R. J. Kieber, D. J. Kieber, R. J. Sikorski and R. D. Jones, *Nature*, 1991, **353**, 60-62.
53. P. Schmitt-Kopplin, N. Hertkorn, H.-R. Schulten and A. Kettrup, *Environ. Sci. Technol.*, 1998, **32**, 2531-2541.
54. S. L. H. Sandvik, P. Bilski, J. D. Pakulski, C. F. Chignell and R. B. Coffin, *Mar. Chem.*, 2000, **69**, 139-152.
55. Y. Yamashita, J. N. Boyer and R. Jaffé, *Continental Shelf Research*, 2013, **66**, 136-144.
56. K. Cawley, P. Wolski, N. Mladenov and R. Jaffé, *Wetlands*, 2012, **32**, 475-486.
57. V. H. Rivera-Monroy, R. R. Twilley, S. E. Davis, III, D. L. Childers, M. Simard, R. Chambers, R. Jaffe, J. N. Boyer, D. T. Rudnick, K. Zhang, E. Castaneda-Moya, S. M. L. Ewe, R. M. Price, C. Coronado-Molina, M. Ross, T. J. Smith, III, B. Michot, E. Meselhe, W. Nuttle, T. G. Troxler and G. B. Noe, *Critical Reviews in Environmental Science and Technology*, 2011, **41**, 633-669.
58. J. R. Helms, A. Stubbins, J. D. Ritchie, E. C. Minor, D. J. Kieber and K. Mopper, *Limnol Oceanogr*, 2008, **53**, 955-969.
59. J. L. Weishaar, G. R. Aiken, B. A. Bergamaschi, M. S. Fram, R. Fujii and K. Mopper, *Environ. Sci. Technol.*, 2003, **37**, 4702-4708.
60. C. A. Stedmon, S. Markager and R. Bro, *Mar. Chem.*, 2003, **82**, 239-254.
61. C. A. Stedmon and R. Bro, *Limnology and Oceanography-Methods*, 2008, **6**, 572-579.
62. S. E. Page, W. A. Arnold and K. McNeill, *Journal of Environmental Monitoring*, 2010, **12**, 1658-1665.
63. G. Buxton, C. Greenstock, W. P. Helman and A. Ross, *J. Phys. Chem. Ref. Data*, 1988, **17**, 513.
64. T. Z. Osborne, G. L. Brunland, S. Newman, K. R. Reddy and S. Grunwald, *Environmenal Monitoring & Assessment*, 2011, **183**, 395-408.

65. W. R. Haag, J. Hoigne, E. Gassman and A. M. Braun, *Chemosphere*, 1984, **13**, 631-640.
66. M. A. J. Rodgers and P. T. Snowden, *Journal of the American Chemical Society*, 1982, **104**, 5541-5543.
67. M. Minella, F. Romeo, D. Vione, V. Maurino and C. Minero, *Chemosphere*, 2011, **83**, 1480-1485.
68. J. E. Grebel, J. J. Pignatello and W. A. Mitch, *Water Res.*, 2011, **45**, 6535-6544.
69. K. M. Parker, J. J. Pignatello and W. A. Mitch, *Environ. Sci. Technol.*, 2013, **47**, 10987-10994.
70. B. A. Cottrell, S. A. Timko, L. Devera, A. K. Robinson, M. Gonsior, A. E. Vizenor, A. J. Simpson and W. J. Cooper, *Water Res.*, 2013, **47**, 5189-5199.
71. B. J. Dalzell, E. C. Minor and K. M. Mopper, *Organic Geochemistry*, 2009, **40**, 243-257.
72. M. Grandbois, D. E. Latch and K. McNeill, *Environ. Sci. Technol.*, 2008, **42**, 9184-9190.
73. C. M. Glover and F. L. Rosario-Ortiz, *Environ. Sci. Technol.*, 2013, **47**, 13949-13956.
74. L. Cavani, S. Halladja, A. ter Halle, G. Guyot, G. Corrado, C. Ciavatta, A. Boulkamh and C. Richard, *Environ. Sci. Technol.*, 2009, **43**, 4348-4354.
75. C. Richard, O. Trubetskaya, O. Trubetskoj, O. Reznikova, G. Afanas'eva, J. P. Aguer and G. Guyot, *Environ. Sci. Technol.*, 2004, **38**, 2052-2057.
76. E. Lee, C. M. Glover and F. L. Rosario-Ortiz, *Environ. Sci. Technol.*, 2013.
77. S. Mostafa and F. L. Rosario-Ortiz, *Environ. Sci. Technol.*, 2013, **47**, 8179-8186.
78. K. S. Golanoski, S. Fang, R. Del Vecchio and N. V. Blough, *Environ. Sci. Technol.*, 2012, **46**, 3912-3920.
79. C. M. Sharpless, *Environ. Sci. Technol.*, 2012, **46**, 4466-4473.
80. V. Maurino, A. Bedini, D. Borghesi, D. Vione and C. Minero, *Phys Chem Chem Phys*, 2011, **13**, 11213-11221.
81. J. Ma, R. Del Vecchio, K. S. Golanoski, E. S. Boyle and N. V. Blough, *Environ. Sci. Technol.*, 2010, **44**, 5395-5402.
82. S. E. Page, J. R. Logan, R. M. Cory and K. McNeill, *Environmental Science: Processes & Impacts*, 2014. DOI: 10.1039/C3EM00596H
83. Y. Zhang, R. Del Vecchio and N. V. Blough, *Environ. Sci. Technol.*, 2012, **46**, 11836-11843.

Table 1: Site information and water quality analysis of sample sites

Station	Latitude °N	Longitude °W	Salinity	pH	DOC (mg L^{-1})	Total Alkalinity (mg $CaCO_3$ L^{-1})
H1	25.43798	80.9513	2.30	7.11	19.34	278.2
H2	25.41641	80.99297	8.03	7.51	17.80	295.4
H3	25.42352	81.05861	17.19	7.47	16.36	308.2
H4	25.43184	81.09126	26.63	7.40	13.87	293.8
H5	25.42671	81.1148	33.89	7.68	8.98	244.4
H6	25.38675	81.16042	37.96	7.94	6.37	217.6
T1	25.19582	80.63785	11.15	7.80	14.43	217.3
T2	25.20554	80.64632	19.82	8.00	12.26	210.2
T3	25.20044	80.64553	23.87	8.09	11.45	207.9
T4	25.17505	80.6292	27.17	8.15	8.86	192.7
T5	25.11645	80.72102	35.25	8.09	9.26	180.2
T6	25.01301	80.69453	37.37	8.15	5.74	171.3

Table 2: Optical Properties and PARAFAC

Site	S_R	$a_{CDOM}(254)$ (m^{-1})	$SUVA_{254}$ ($L \cdot m^{-1} \cdot mg\ C^{-1}$)	C1 (QSU)	C2 (QSU)	C3 (QSU)	C4 (QSU)	C5 (QSU)	C6 (QSU)	C7 (QSU)	C8 (QSU)	Total Fluor (QSU)
H1	5.04	138.65	3.11	224.62	84.12	105.84	85.92	102.81	57.28	24.37	24.37	709.32
H2	4.95	135.69	3.31	189.59	70.98	75.17	72.83	87.58	53.05	21.22	22.02	592.43
H3	4.61	144.38	3.83	192.04	59.10	72.17	66.85	92.07	50.52	20.62	18.87	572.24
H4	4.57	118.41	3.71	153.07	33.06	56.89	50.86	74.53	39.18	14.77	13.95	436.31
H5	4.92	70.47	3.41	80.81	15.55	28.71	30.21	38.95	23.24	10.61	9.17	237.25
H6	6.52	34.26	2.33	30.39	10.55	11.11	15.18	14.77	9.74	6.40	5.22	103.36
T1	6.60	80.69	2.43	66.25	20.45	30.40	31.51	31.93	17.94	21.20	12.79	232.47
T2	7.43	56.84	2.01	39.22	16.35	14.47	21.23	21.24	12.99	14.57	8.29	148.37
T3	9.46	40.90	1.55	25.29	14.59	6.26	15.35	12.30	9.81	11.73	6.30	101.64
T4	13.77	26.81	1.31	13.88	10.26	1.57	9.64	6.67	6.37	10.51	4.69	63.58
T5	13.65	28.32	1.33	15.21	10.12	2.49	11.25	6.01	7.54	13.54	5.89	72.06
T6	8.94	13.19	1.00	7.25	3.37	0.65	4.40	3.09	3.60	7.89	2.77	33.02

Table 3: Reactive species formation rates and steady-state concentrations

Site	$^1O_2$		$^3DOM^*$		$CO_3^{\cdot-}$		·OH	
	R ($x10^8$ M s^{-1})	[SS] ($x10^{14}$ M)	*R* ($x10^8$ M s^{-1})	[SS] ($x10^{15}$ M)	*R* ($x10^{12}$ M s^{-1})	[SS] ($x10^{16}$ M)	*R* ($x10^{12}$ M s^{-1})	[SS] ($x10^{17}$ M)
H1	9.76 ± 0.07	39.0 ± 0.3	9.45 ± 0.64	25.8 ± 8.2	42.6 ± 1.2	78.7 ± 25.4	44.9 ± 2.2	15.1 ± 2.7
H2	10.2 ± 0.9	41.0 ± 3.7	10.6 ± 0.5	25.1 ± 14.5	25.5 ± 0.3	51.2 ± 16.5	22.5 ± 0.2	8.01 ± 1.41
H3	8.48 ± 0.28	33.9 ± 1.1	6.05 ± 0.14	23.9 ± 7.3	20.1 ± 0.4	43.9 ± 14.1	18.3 ± 0.5	7.04 ± 1.25
H4	6.79 ± 0.51	27.2 ± 2.0	6.60 ± 0.14	33.8 ± 10.2	11.9 ± 0.5	30.6 ± 9.9	11.5 ± 0.3	5.14 ± 0.91
H5	4.36 ± 0.56	17.4 ± 2.2	3.48 ± 0.18	26.4 ± 8.3	5.06 ± 0.26	20.1 ± 6.6	5.58 ± 0.16	3.70 ± 0.66
H6	2.80 ± 0.28	11.2 ± 1.1	3.69 ± 0.18	12.0 ± 3.7	1.28 ± 0.02	7.20 ± 2.32	1.44 ± 0.10	1.27 ± 0.24
T1	5.13 ± 0.18	20.5 ± 0.7	4.02 ± 0.25	20.7 ± 6.6	8.82 ± 0.15	21.8 ± 7.0	10.5 ± 0.2	4.65 ± 0.82
T2	3.43 ± 0.10	13.7 ± 0.4	5.17 ± 0.47	13.9 ± 4.6	6.44 ± 0.25	18.8 ± 6.1	6.31 ± 0.14	3.15 ± 0.56
T3	2.62 ± 0.11	10.5 ± 0.4	4.96 ± 0.52	12.4 ± 4.3	2.76 ± 0.08	8.61 ± 2.78	3.10 ± 0.05	1.67 ± 0.29
T4	1.94 ± 0.18	7.74 ± 0.73	2.80 ± 0.27	10.0 ± 3.4	1.82 ± 0.06	7.36 ± 2.38	2.09 ± 0.09	1.41 ± 0.26
T5	2.04 ± 0.26	8.16 ± 1.06	2.33 ± 0.08	12.7 ± 3.9	1.11 ± 0.12	4.29 ± 1.46	1.41 ± 0.02	0.93 ± 0.16
T6	0.90 ± 0.16	3.61 ± 0.63	1.86 ± 0.10	6.07 ± 1.87	0.41 ± 0.04	2.58 ± 0.87	0.55 ± 0.16	0.55 ± 0.18

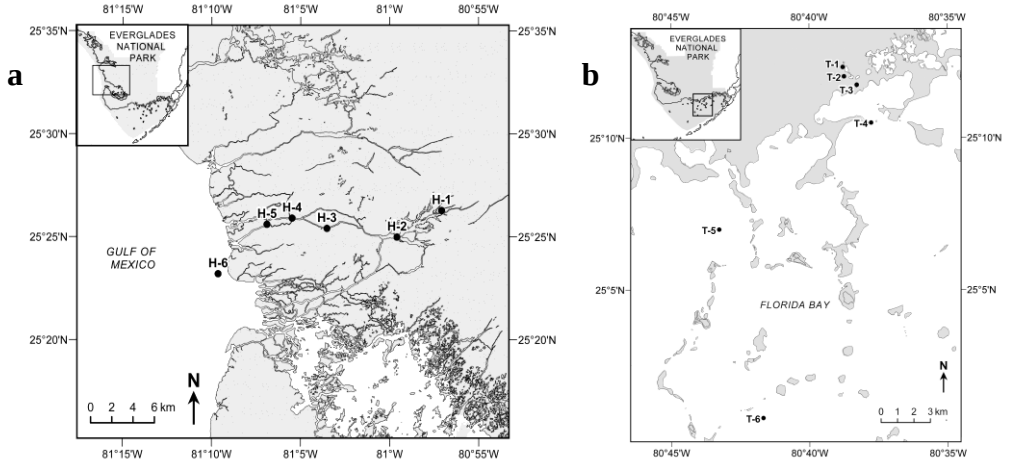

Figure 1: Sample site locations in Everglades National Park, Florida, USA (a) Harney River sample sites in the Shark River Slough, and (b) Taylor River and Florida Bay samples in the Taylor Slough.

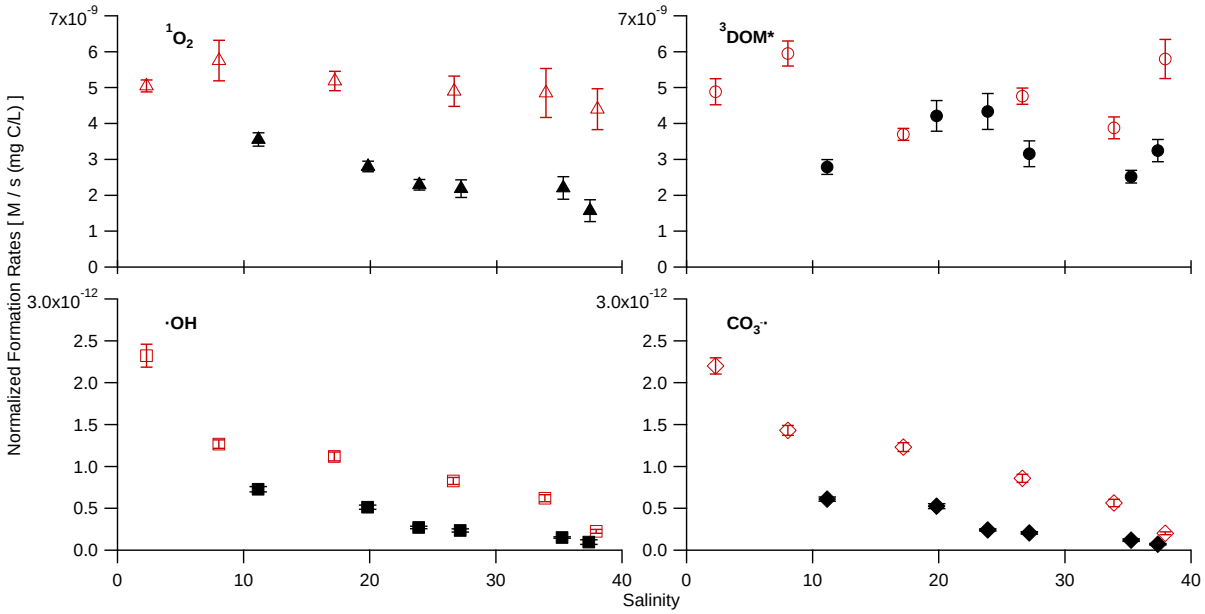

Figure 2: Normalized formation rates of (a) $^1O_2$ (triangles), (b) ^{3}DOM* (circles), (c) •OH (squares) and (d) $CO_3^{-\bullet}$ (diamonds) across transects of the Harney River (red, open) and Taylor Slough (black, filled). Error bars represent standard deviations of triplicate experiments for $^1O_2$, •OH, and $CO_3^{-\bullet}$. ^{3}DOM* error bars are calculated from standard deviations of the regression analysis (Equation 8).

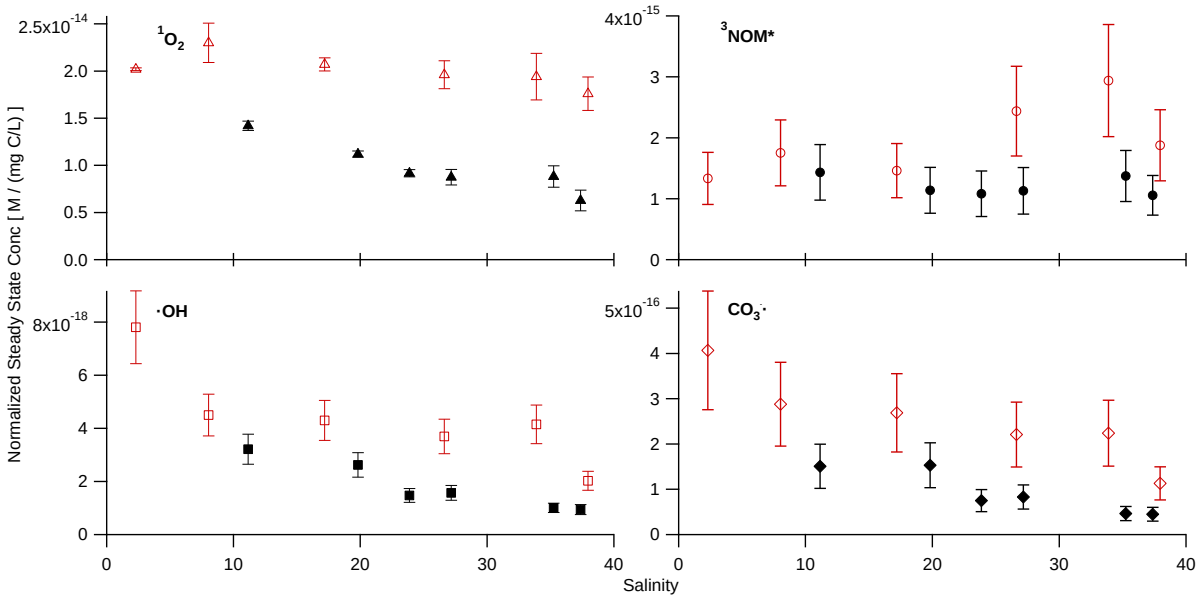

Figure 3: Normalized steady-state concentrations of (a) $^1O_2$ (triangles), (b) ^{3}DOM* (circles), (c) •OH (squares) and (d) $CO_3^{-\bullet}$ (diamonds) across transects of the Harney River (red, open) and Taylor Slough (black, filled). Error bars represent standard deviations of triplicate experiments for $^1O_2$, •OH, and $CO_3^{-\bullet}$. ^{3}DOM* error bars are calculated from standard deviations of the regression analysis (Equation 8).

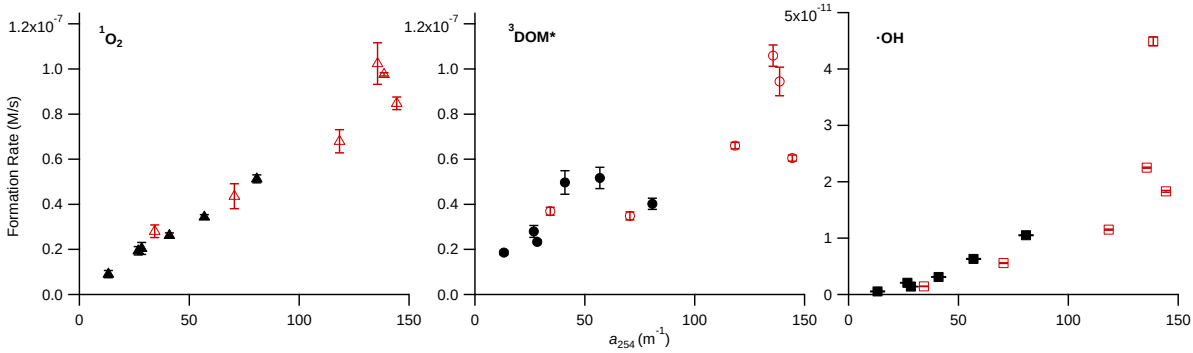

Figure 4: Formation rates of (a) $^1O_2$ (triangles) and (b) ^{3}DOM* (circles), and (c) •OH (squares) in relation to the absorbance at 254 nm, a_{254}, of the Harney River (red, open) and Taylor Slough (black, filled). Error bars represent standard deviations of triplicate experiments for $^1O_2$, •OH, and $CO_3^{-\bullet}$. ^{3}DOM* error bars are calculated from standard deviations of the regression analysis (Equation 8).

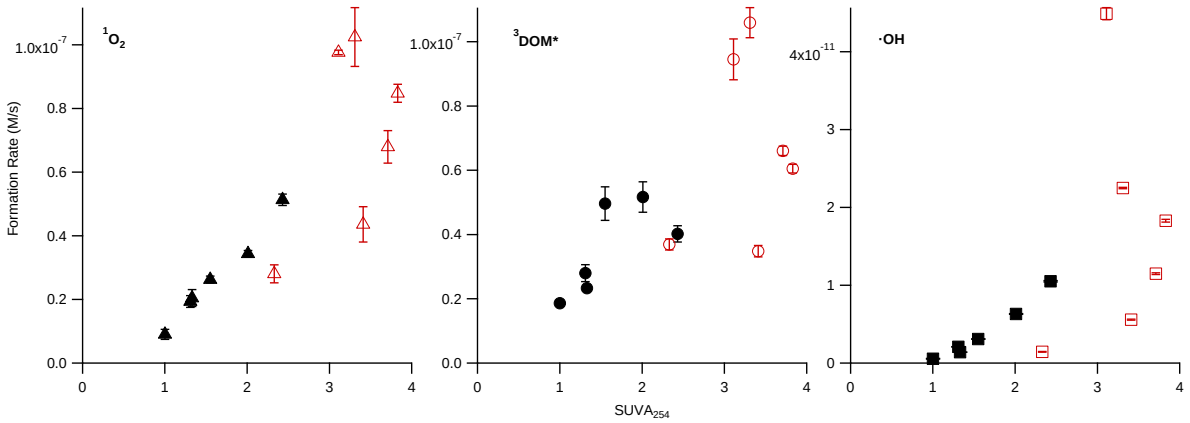

Figure 5: Formation rates of (a) $^1O_2$ (triangles) and (b) ^{3}DOM* (circles), (c) •OH (squares) and (d) $CO_3^{-\bullet}$ (diamonds) in relation to $SUVA_{254}$ of the Harney River (red, open) and Taylor Slough (black, filled). Error bars represent standard deviations of triplicate experiments for $^1O_2$, •OH, and $CO_3^{-\bullet}$. ^{3}DOM* error bars are calculated from standard deviations of the regression analysis (Equation 8).

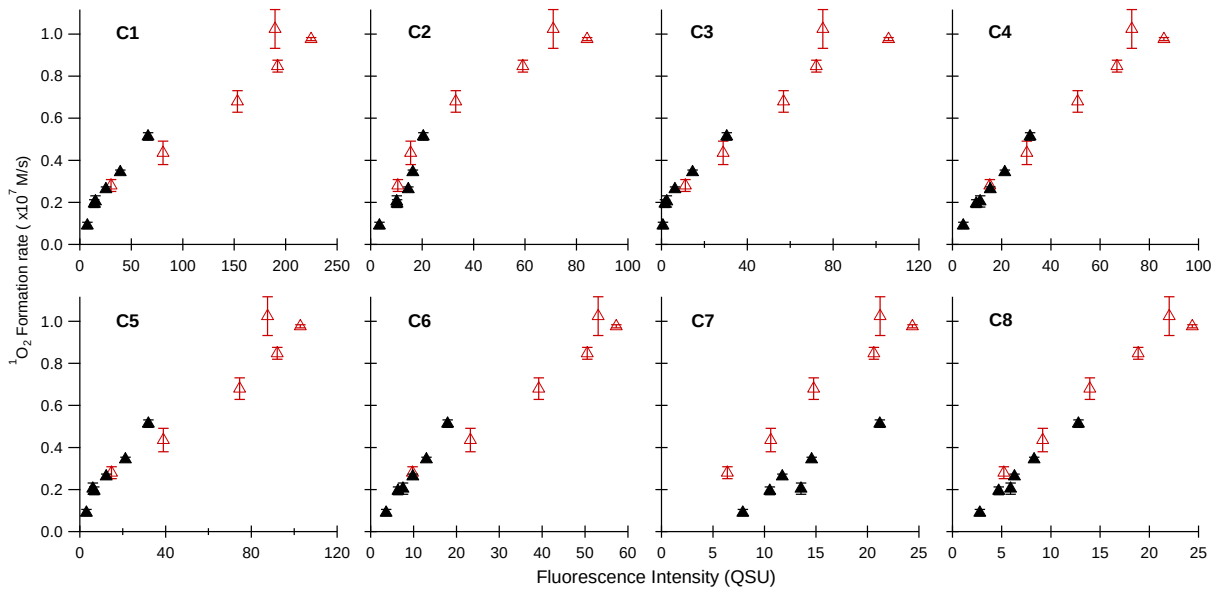

Figure 6: Formation rates of $^1O_2$ in the Harney River (red, open) and Taylor Slough (black, filled) as related to fluorescence intensity (QSU) of the different DOM components as identified by PARAFAC analysis. Error bars represent standard deviations of triplicate experiments

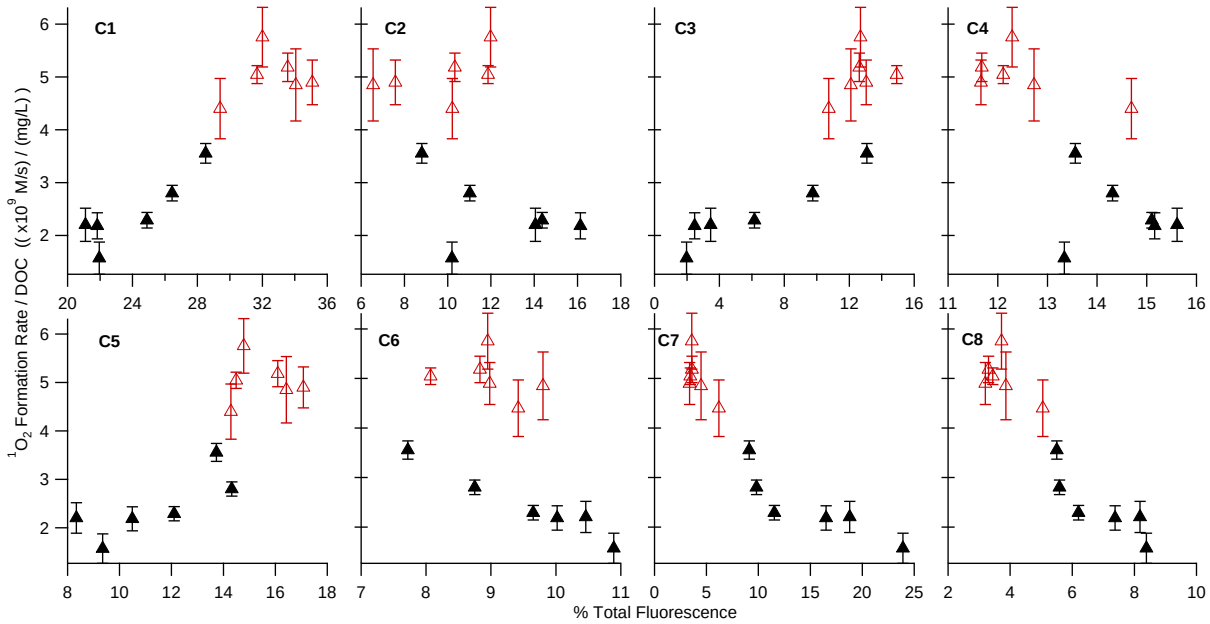

Figure 7: Normalized formation rates of $^1O_2$ in the Harney River (red, open) and Taylor Slough (black, filled) as related to percent total fluorescence intensity of the different DOM components as identified by PARAFAC analysis. Error bars represent standard deviations of triplicate experiments